Three-Dimensional Nonequilibrium Viscous Shock-Layer Flow over the Space Shuttle Orbiter

M.D. Kim,* S. Swaminathan,* and Clark H. Lewis†
Virginia Polytechnic Institute and State University, Blacksburg, Virginia

A numerical method has been developed to predict the three-dimensional nonequilibrium flowfield past the Space Shuttle Orbiter at high angle of attack. An existing viscous shock-layer method has been extended to include finite-rate chemical reactions of multicomponent ionizing air. A general nonorthogonal computational grid system was introduced to treat the nonaxisymmetric geometry. At Shuttle re-entry flight conditions, nonequilibrium real gas effects on the surface-measurable quantities are significant. The present method can predict the nonequilibrium flowfield over the entire windward surface of the Shuttle Orbiter at high angle of attack (up to 50 deg). The computational results obtained show good agreement compared to the STS-2 flight data and other numerical solutions.

Nomenclature

C_i = concentration of species i, ρ_i/ρ
C_p = specific heat at constant pressure
g = determinant of coordinate metric tensor
g_{ij} = coordinate metric tensor, $\boldsymbol{g}_i \cdot \boldsymbol{g}_j$; $i,j = 1,2,3$
$\boldsymbol{g}_1$ = vector in streamwise (ξ_1) direction
$\boldsymbol{g}_2$ = vector in normal (ξ_2) direction
$\boldsymbol{g}_3$ = vector in circumferential (ξ_3) direction
h = static enthalpy, h^*/U_∞^2
k = thermal conductivity, $k^*/(\mu_{\text{ref}} C_{p\infty})$
L = Shuttle body total length, 32.84 m
Le = Lewis number
M_i = species molecular weight
$\bar{M}$ = mixture molecular weight, $1/(\Sigma C_i/M_i)$
M_∞ = freestream Mach number
n_{sh} = shock standoff distance, n_{sh}^*/R_n
NS = number of species
NONEQL = nonequilibrium flow solution
p = pressure, $p^*/(\rho_\infty U_\infty^2)$
Pr = Prandtl number, $C_p^* \mu^*/k^*$
Q_w = heating rate due to conduction and diffusion, MW/m^2
R = universal gas constant
Re_∞ = freestream unit Reynolds number, m^{-1}
R_n = dimensional Shuttle nose radius, 62.23 cm (24.5 in.)
SHTNEQ = Shuttle nonequilibrium, the present numerical method
STS = Space Transportation System
T = temperature, T^*/T_{ref}
T_{ref} = dimensional reference temperature, $U_\infty^2/C_{p\infty}$
t = Shuttle entry time from 122 km altitude interface
u,v,w = streamwise, normal, and circumferential velocity tensor components non-dimensionalized by U_∞
U_∞ = dimensional freestream velocity
$\dot{w}_i$ = species production term
z,r,ϕ = reference cylindrical coordinates
α = angle of attack, deg
ϵ = Reynolds number parameter, $\epsilon^2 = \mu_{\text{ref}}/(\rho_\infty U_\infty R_n)$
γ = ratio of specific heats
μ = viscosity, μ^*/μ_{ref}
μ_{ref} = reference viscosity evaluated at T_{ref}
ξ_1,ξ_2,ξ_3 = body-generator computational coordinates
η = normalized normal coordinate, ξ_2/n_{sh}
ρ = density, ρ^*/ρ_∞
σ = shock angle with respect to freestream velocity vector

Superscripts

$(\ )^*$ = dimensional quantity
$\bar{(\ )}$ = quantity normalized by shock value
$\hat{(\ )}$ = quantity along shock-normal coordinates

Subscripts

i = species i
ref = dimensional reference quantity
sh = value behind the shock
w = wall value
∞ = dimensional freestream value

Introduction

In recent years, various numerical methods have been applied to solve the nonequilibrium viscous flowfield over the windward surface of the Space Shuttle during re-entry. For instance, Miner and Lewis[1] developed a two-dimensional nonequilibrium viscous shock-layer method and applied it to the flowfield solution for the windward plane of the Space Shuttle Orbiter using an "equivalent axisymmetric body" concept. Shinn et al.[2] analyzed the finite catalytic wall effect on the Shuttle windward plane heating using a two-dimensional nonequilibrium viscous shock-layer method. Rakich and Lanfranco[3] used a more approximate axisymmetric analog of a boundary-layer method to solve the nonequilibrium flow over the Shuttle windward surface. Rakich et al.[4] also performed an analysis to investigate the catalytic efficiency of the Space Shuttle heat shield and determined that the heat shield tiles are almost noncatalytic. Scott and Derry[5] calculated the Shuttle windward centerline heating by combining the three-dimensional inviscid flow solutions with reacting two-dimensional axisymmetric analog boundary-layer calculations including the finite catalytic wall effect. They also discussed some possible reasons for the overprediction of the calculated results on the forward part of

Presented as Paper 83-0487 at the AIAA 21st Aerospace Sciences Meeting, Reno, Nev., Jan. 10-13, 1983; submitted Feb. 22, 1983; revision received June 27, 1983.

*Graduate Student, Aerospace and Ocean Engineering Department. Student Member AIAA.

†Professor, Aerospace and Ocean Engineering Department. Associate Fellow AIAA.

the body. However, none of the foregoing could solve the three-dimensional reacting viscous flowfield at high angle of attack without a major approximation such as the axisymmetric analog.

The purpose of the present work is to develop a numerical method to predict the three-dimensional nonequilibrium viscous flowfield past the Space Shuttle at high angle of attack. An existing viscous shock-layer method[6] has been extended to include finite-rate chemical reactions of multicomponent ionizing air. It is assumed that the chemical reactions proceed at a finite rate, and a chemical model which includes seven species and seven reaction equations is used to calculate the rate of production terms. The reaction equations and reaction rate constants are taken from Blottner et al.[7] A general nonorthogonal computational grid system was introduced to treat the nonaxisymmetric Shuttle geometry. This coordinate system is similar to the one defined by Helliwell et al.,[8] except that the second coordinate ξ_2 of the present system is a straight line in the body-normal direction. The three velocity components are tensor quantities and are defined in the nonorthogonal coordinate directions. Since the viscous shock-layer equations are parabolic in both the streamwise and crossflow directions, the equations are solved by a highly efficient finite difference scheme,[9] which requires much less computing time than parabolized Navier-Stokes (PNS) or time-dependent methods. The present method can solve both subsonic and supersonic flows and requires the shock shape as input data. The shock shapes for the present Shuttle calculations were provided by the inviscid HALIS method.[10]

In the later sections, the governing equations and boundary conditions are presented, and the thermodynamic properties and chemical reaction model are described also. It is known that the nonequilibrium real gas effects persist through a wide range of the Shuttle re-entry trajectory (altitudes from 122 to 50 km). In the present work, three points along the trajectory of the second Space Shuttle flight (STS-2) are chosen, and the numerical solutions are obtained over the entire windward surface of the body. The computational results of the surface heating rate are compared with the STS-2 flight data, and the surface pressure results are compared with the inviscid HALIS solutions. The comparisons show good agreement. The variations of some shock-layer profiles along the body are also presented.

Analysis

Governing Equations

The governing equations are derived from the steady Navier-Stokes equations for a reacting gas mixture as given by Bird et al.,[11] and they are written in a surface-oriented general nonorthogonal coordinate system (see Fig. 1). The ξ_2 coordinate consists of straight lines in the surface-normal direction. At the body surface, the ξ_3 coordinate is set to coincide with the ϕ coordinate of the reference cylindrical coordinate system. The coordinate system requires orthogonality only at the body surface. The normal velocity v and normal coordinate ξ_2 are assumed to be on the order of ϵ, and all terms which are of higher order than ϵ are neglected in the governing equations. The local physical velocity vector is defined as

$$V = ug_1 + vg_2 + wg_3$$

where u, v, and w are tensor velocity components in the computational coordinate system. Only laminar flow is considered in the present analysis. The derived nondimensional form of the three-dimensional viscous shock-layer equations for a reacting gas mixture is given in Appendix A.

Boundary Conditions

At the body surface, the no-slip and no-temperature-jump boundary conditions are used. The calculated Reynolds number parameter ϵ was less than 0.108 for the present test cases, which indicates that the slip effects will not be important (see, e.g., Davis[12]). The wall temperature is specified by the STS-2 flight thermocouple data. Recently it has been shown that the Space Shuttle thermal protection tiles are almost noncatalytic.[4] In the present calculations, the wall species concentrations are dictated by the noncatalytic condition, but the boundary condition can be extended easily to include the effects of finite wall catalycity to the recombination of dissociated air.

In the present method, shock shape information is necessary as an input which is used for the calculation of the shock-boundary condition. The three-dimensional shock-boundary conditions with slip effects (modified Rankine-Hugoniot jump relations) given by Murray and Lewis[9] have been extended to include finite-rate chemistry and the nonorthogonal coordinate system. Two-dimensional shock-normal coordinates are defined in the plane which contains both the freestream velocity vector and the vector which is normal to the local shock surface. Then the freestream velocity vector is written in the shock-normal coordinates, and two-dimensional shock crossing is calculated in the shock-normal coordinates. The nonequilibrium shock-crossing relations written in the shock-normal coordinates are presented in Appendix B. The known after-shock quantities are rotated into the three-dimensional computational coordinates.

Thermodynamic and Transport Properties

Multicomponent ionizing air is considered to be a mixture of thermally perfect gases, and the thermodynamic and transport properties for each species are calculated using the local temperature. The properties for the gas mixture are then determined in terms of the individual species properties. The enthalpy and specific heat of each species are obtained from the thermodynamic data tabulated by Browne.[13-15] The second-order Lagrangian method is used to interpolate the values for a given temperature. The viscosity of the individual species is calculated from the curve fit relation given by Blottner,[16] and the thermal conductivity of each species is calculated from the Eucken semi-empirical formula using the species viscosity and specific heat. After the viscosity and thermal conductivity of the individual species are calculated, the viscosity and thermal conductivity of the gas mixture are calculated from the method suggested by Armaly and Sutton.[17,18] In the present work, the diffusion model is limited to binary diffusion with the binary diffusion coefficient specified by the Lewis number of 1.4.

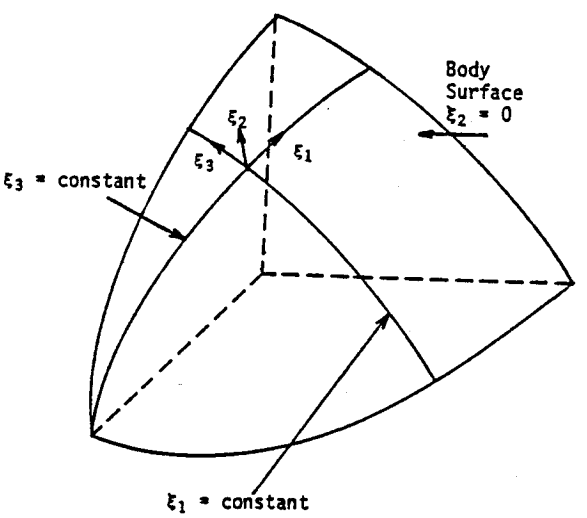

Fig. 1 Body-generator nonorthogonal coordinate system.

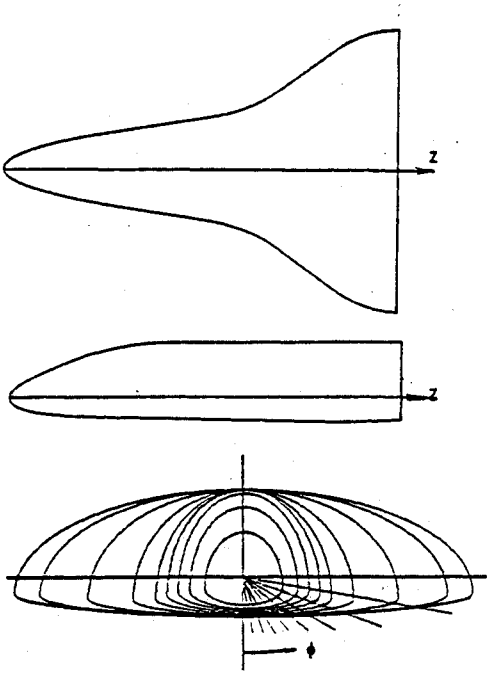

Fig. 2 Cross sections of the modified Shuttle Orbiter.

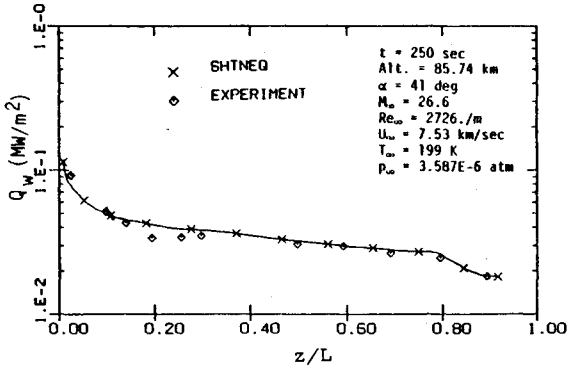

Fig. 3 Comparison of measured and calculated heating rates at $\phi = 0$ for case 1.

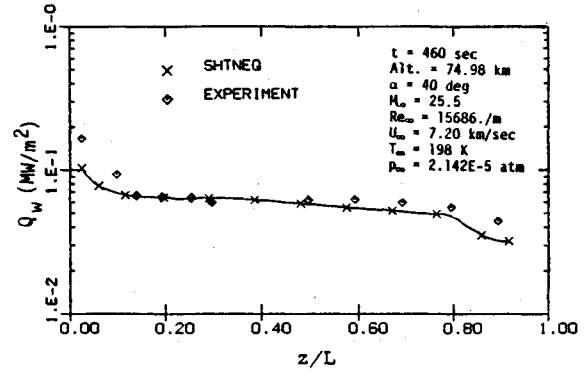

Fig. 4 Comparison of measured and calculated heating rates at $\phi = 0$ for case 2.

Chemical Reaction Model

It is assumed that the chemical reactions proceed at a finite rate, and the rate of production terms $\dot{w}_i$ of the individual species are included in the energy equation and the species continuity equations. The $\dot{w}_i$ terms are function of both temperature and species concentrations, and they need to be rewritten so that the temperature or the species concentrations appears as one of the unknowns, as given in Ref. 1. In the present calculations, the chemical reaction model and the reaction-rate constants are taken from Blottner.[7] Seven chemical species are considered in the reactions; viz., O, O_2, NO, N, NO^+, N_2, and e^-. The following pure air chemical reactions are used for the present study.

1) $O_2 + M_1 \rightarrow 2O + M_1$
2) $N_2 + M_2 \rightarrow 2N + M_2$
3) $N_2 + N \rightarrow 2N + N$
4) $NO + M_3 \rightarrow N + O + M_3$
5) $NO + O \rightarrow O_2 + N$
6) $N_2 + O \rightarrow NO + N$
7) $N + O \rightarrow NO^+ + e^-$

where M_1, M_2, and M_3 are the catalytic third bodies.[7] Since the rate of production terms is for nonequilibrium flows, the present method encounters difficulty in obtaining a converged solution whenever the flow conditions approach equilibrium. The difficulty is severe particularly at the stagnation point.

Numerical Solution

Davis[12] presented an implicit finite-difference method to solve the viscous shock-layer equations for axially symmetric flows, and Murray and Lewis[9] further developed the scheme for three-dimensional flows. In the present work, the method is extended to the chemically reacting three-dimensional flowfield solution in a surface-oriented nonorthogonal coordinate system. Since the viscous shock-layer equations are parabolic in both the streamwise and crossflow directions, the equations are solved by a highly efficient finite-difference scheme. The continuity and normal momentum equations are solved in a coupled form to promote convergence. The pressure and the normal velocity are obtained by solving the coupled equations simultaneously. This method of coupling helps convergence, especially for expanding flow regions. The shock standoff distance is evaluated by integrating the continuity equation.

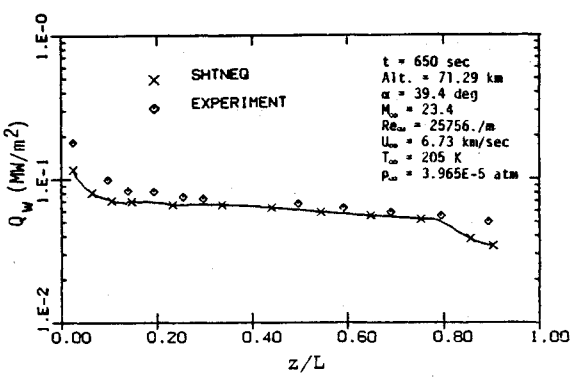

Fig. 5 Comparison of measured and calculated heating rates at $\phi = 0$ for case 3.

Table 1 Test case freestream conditions

Case No	t, s	Altitude, km	α, deg	M_∞	Re_∞, m^{-1}	U_∞, km/s	T_∞, K	p_∞, atm
1	250	85.74	41.0	26.6	2,726	7.53	199	$3.587E-06$
2	460	74.98	40.0	25.5	15,686	7.20	198	$2.142E-05$
3	650	71.29	39.4	23.4	25,756	6.73	205	$3.965E-05$

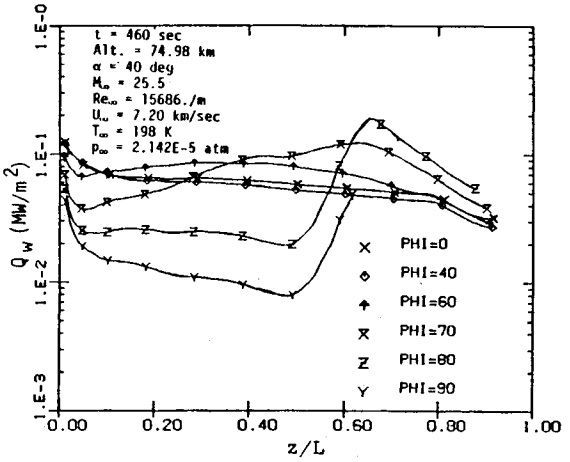

Fig. 6 Surface heating-rate distributions along the body for case 2.

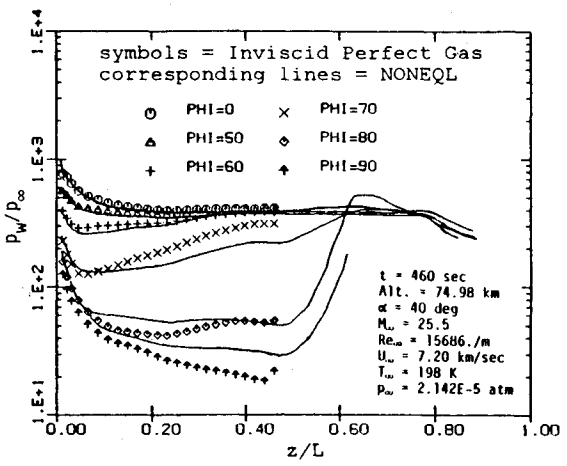

Fig. 8 Comparison of surface pressure along the body with inviscid HALIS results for case 2.

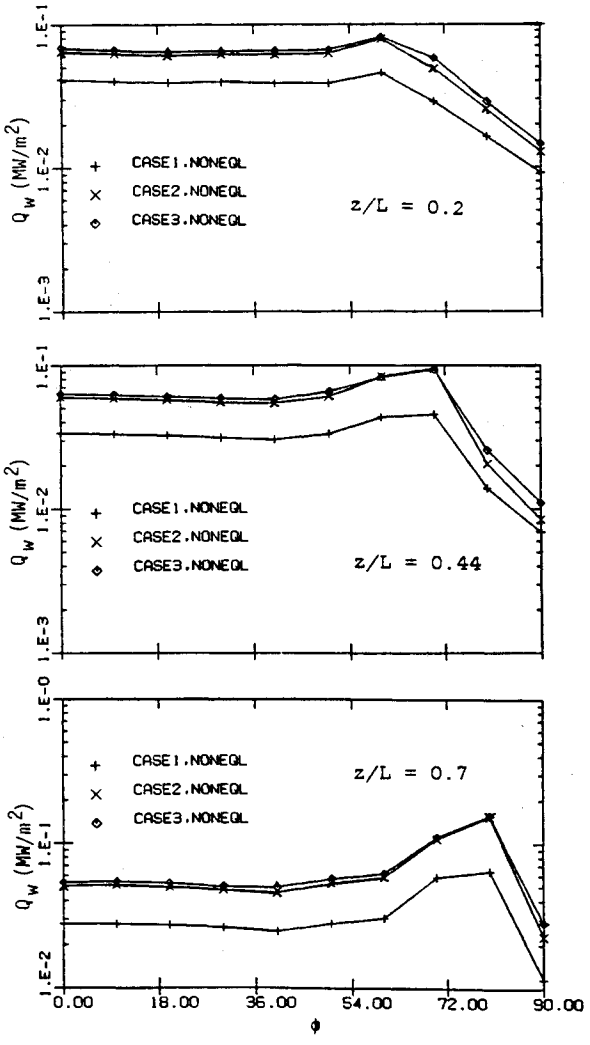

Fig. 7 Spanwise heating-rate distributions at various locations for each case.

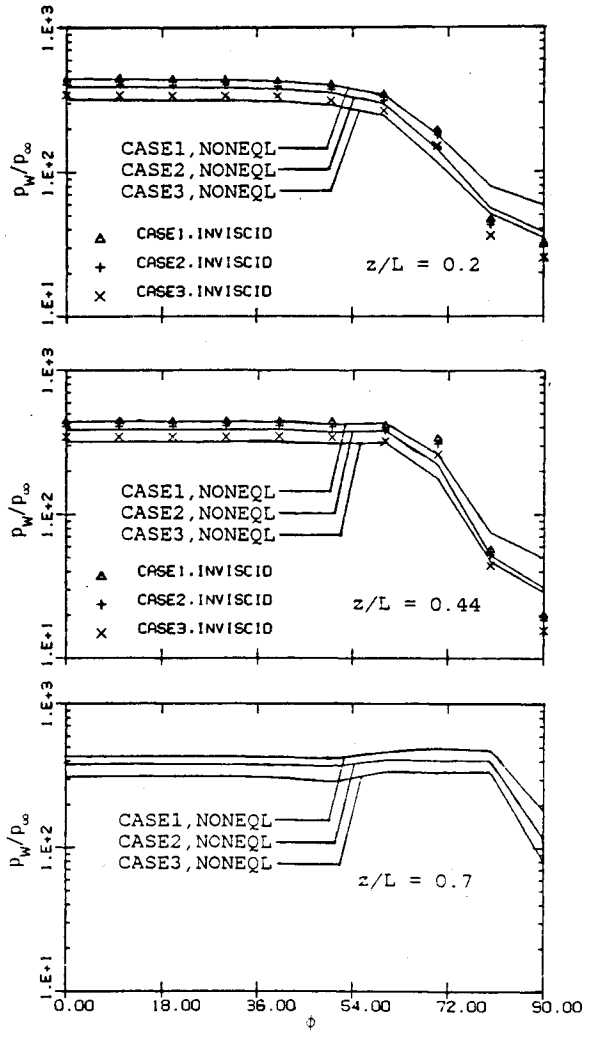

Fig. 9 Comparison of surface pressure around the body at various locations for each case.

Results and Discussion

In order to validate the developed SHTNEQ (Shuttle-nonequilibrium) code, three points along the second Space Shuttle trajectory (STS-2) have been chosen and complete windward flowfield solutions have been obtained. For the wide range of the Shuttle re-entry conditions (above 50 km altitude), nonequilibrium effects can occur. The nonequilibrium effects are greatest near the nose of the body and around $t=450$ s on the trajectory.[4] The altitudes selected for the present calculations are 81, 70, and 60 km ($t=250$, 460, 630 s, respectively). Detailed freestream conditions for the three test cases are given in Table 1. The cross sections of the modified Shuttle Orbiter which have been used for the inviscid and viscous solutions are depicted in Fig. 2. This geometry is identical to the one used by Weilmuenster and Hamilton.[10] For the windward surface, the geometry data (numerical table) accurately represent the actual nonanalytic

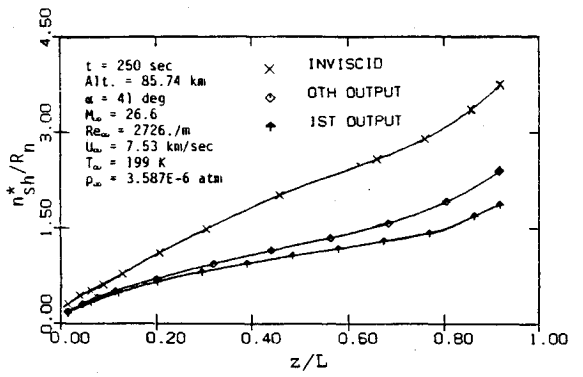

Fig. 10 Comparison of shock-layer thickness between global iterations for case 1.

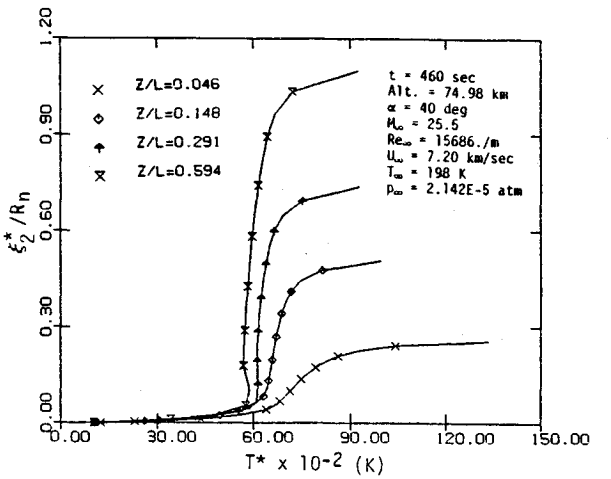

Fig. 11 Shock-layer profiles of temperature at various body locations along $\phi = 0$ for case 2.

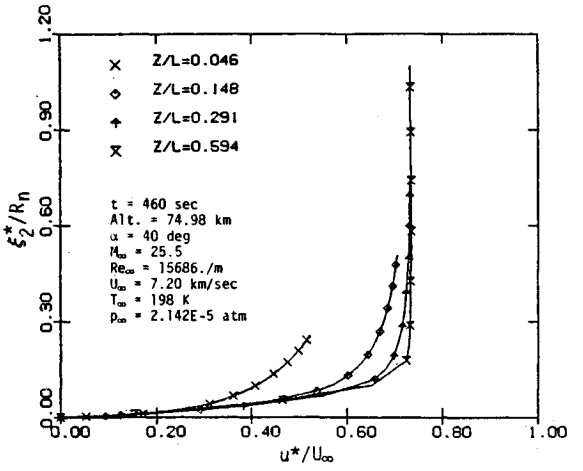

Fig. 12 Shock-layer profiles of velocity at various body locations along $\phi = 0$ for case 2.

Shuttle geometry. For the leeward surface, an artificially smoothed surface is used in order to obtain an inviscid solution of shock data. Presented results include the surface heating rate, surface pressure, shock shapes, and a few shock-layer profiles. The flight heating-rate data obtained from the method by Throckmorton[19] are used for comparison with the computational results. The inviscid pressure calculations by the HALIS code[10] are used for comparison with the present surface-pressure results.

In Figs. 3-5, comparisons of surface heating along the body with the flight measurement data are presented; the agreement is quite good at most stations. The reason for the local mismatch near $z/L = 0.2$ for case 1 is not currently known, but it may be due to the flight data uncertainty (10%).[19] On the nose region and the trailing edge for cases 2 and 3, the underprediction of the present solution may be due to the effect of finite surface catalycity as indicated in Ref. 4. In fact, the surface catalytic effect for case 1 is negligible compared to that for cases 2 and 3 due to the altitude dependence of the surface catalytic activity. Due to the low density at high altitudes the catalytic recombination of the dissociated particles becomes less effective. This effect can also be observed in Ref. 2. For case 3, the present solution underpredicts about 10% compared to the flight-experiment data. The decrease of the heating after $z/L = 0.8$ is due to the slope change of the body surface. In Fig. 6 the surface heating distributions along the body for all the ϕ planes are shown. The sudden increase of the heating rate at $\phi = 80$ deg and $z/L = 0.5$ is due to the spanwise slope change of the body surface along the body (see Fig. 2). At $z/L = 0.6$ and $\phi = 90$ deg, the solution did not converge, due to the severe surface slope change of the wing tip section. The calculated windward spanwise heating at various axial stations for case 2 is shown in Fig. 7. The problems of oscillatory results in the quasi-three-dimensional approach of Ref. 3 have disappeared in the present solutions.

In Fig. 8 the surface-pressure distribution over the entire Shuttle windward surface is presented, together with the corresponding inviscid perfect gas solution by the HALIS code,[10] for comparison. The inviscid data were available only up to $z/L = 0.46$ due to the very high angle of attack involved and the expanding wing. The agreement is good for most of the region. For $\phi > 70$ deg agreement is not as good, and for this region the inviscid result may be more accurate, because the inviscid solution used more planes around the body (ξ_3 grid points) considering the existence of the wing. The present SHTNEQ solution used 19 planes while the inviscid HALIS solution used 30 planes around the half-body (from 0 to 180 deg). Including more grid points in the present solution will increase the storage requirement and computing time accordingly. In Fig. 9 the spanwise surface pressure distributions for all of the cases are shown at various axial stations. At $z/L = 0.2$ and 0.44, the present results are compared with the inviscid HALIS results.

The shock-layer thickness distributions along the body in the $\phi = 0$ plane are shown in Fig. 10. The 0th (zeroth) global iteration indicates the present SHTNEQ solution using the inviscid input shock. The 1st (first) global iteration indicates the SHTNEQ solution using the 0th iteration output shock. As shown in the figure, the 0th iteration output shock is quite different from the inviscid input shock. In such a case, a global iteration is necessary in order to refine the entire flowfield solution. Thus, for the present three test cases, all of the results presented are from the first global iteration.

The flowfield structure of the viscous shock layer at a few selected axial stations on the $\phi = 0$ plane is depicted in Figs. 11-14. The profiles include temperature, tangential velocity, and mass fractions of oxygen and nitrogen atoms for case 2 ($t = 460$ s). In Fig. 12, it is observed that the viscous effects are dominant across the entire shock layer especially on the forward part of the body. The mass-fraction profiles of oxygen and nitrogen show the effect of the noncatalytic wall conditions used. The oxygen atom concentration at the wall remains almost constant along the body, while the nitrogen atom concentration is reduced downstream.

The computing times consumed for the present code to solve the entire flowfield over the Shuttle windward surface for cases 1, 2, and 3 are 82, 110, and 112 min, respectively, on an IBM 370/3081 general purpose computer. Case 1 took less computing time because convergence was faster at higher altitude where the flow was more nearly frozen. The corresponding computing times for perfect gas or equilibrium air solutions past the Space Shuttle using a viscous shock-

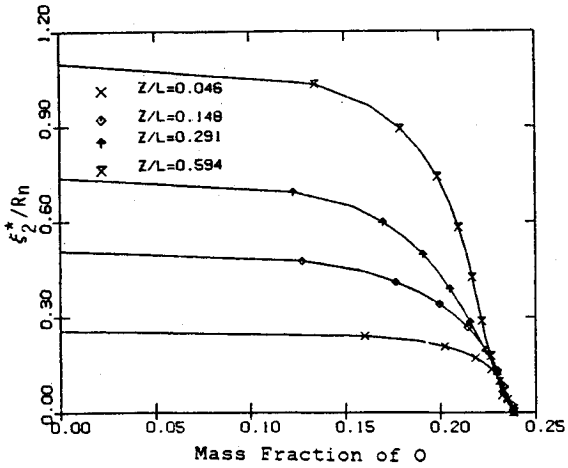

Fig. 13 Shock-layer profiles of oxygen mass fraction at various body locations along $\phi = 0$ for case 2.

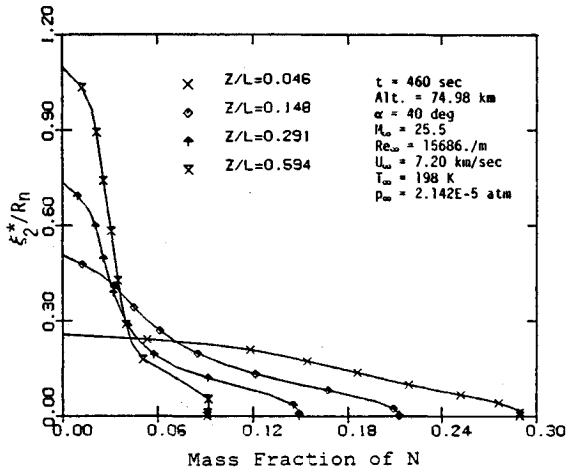

Fig. 14 Shock-layer profiles of nitrogen mass fraction at various body locations along $\phi = 0$ for case 2.

layer method were 31-37 min, as given by Thareja et al.[20] The computing time for a simple sphere-cone (angle of attack of 10 deg and body length of 20 nose radii) using a nonequilibrium viscous shock-layer code which uses an orthogonal coordinate system was typically 26 min, as given by Swaminathan et al.[21] For all of the present test cases, 51 grid points were used in the surface-normal direction, and 19 planes around the body (10 deg step size). The number of marching steps taken along the body (ξ_1 grid points) were 119, 129, and 130, for cases 1, 2, and 3, respectively. The ξ_1 marching step sizes are controlled internally in the code depending upon the number of local iterations taken. The storage requirement of the present SHTNEQ code is 852 kbytes on an IBM 370/3081 computer.

Conclusions

A computational method has been developed to predict the three-dimensional nonequilibrium flowfield past the windward side of the Space Shuttle Orbiter, and numerical solutions were obtained for three different flight conditions. The governing equations take into account the finite-rate chemical reactions of multicomponent ionizing air. A general nonorthogonal computational grid system was introduced to treat the nonaxisymmetric geometry. The present method solved the viscous nonequilibrium flows over the entire Shuttle windward surface in reasonable computing times. The computational results show good agreement compared to the STS-2 flight data and other numerical solutions. In the future the method will be further extended to include more general boundary conditions and chemical models.

Appendix A: Governing Equations

Continuity equation:

$$\frac{\partial}{\partial\xi_1}(\rho u g^{1/2}) + \frac{\partial}{\partial\xi_2}(\rho v g^{1/2}) + \frac{\partial}{\partial\xi_3}(\rho w g^{1/2}) = 0 \tag{A1}$$

u momentum:

$$\rho u\frac{\partial u}{\partial\xi_1} + \rho v\frac{\partial u}{\partial\xi_2} + \rho w\frac{\partial u}{\partial\xi_3} + \rho u^2\begin{Bmatrix}1\\1\ 1\end{Bmatrix} + 2\rho uv\begin{Bmatrix}1\\1\ 2\end{Bmatrix} + 2\rho uw\begin{Bmatrix}3\\1\ 3\end{Bmatrix} + \rho v^2\begin{Bmatrix}3\\2\ 2\end{Bmatrix} + 2\rho vw\begin{Bmatrix}3\\2\ 3\end{Bmatrix} + \rho w^2\begin{Bmatrix}3\\3\ 3\end{Bmatrix} + \frac{g_{22}}{g}\left(g_{33}\frac{\partial p}{\partial\xi_1} - g_{13}\frac{\partial p}{\partial\xi_3}\right) = \frac{\epsilon^2}{g_{22}}\left(\frac{\partial\mu}{\partial\xi_2}\frac{\partial u}{\partial\xi_2} + \mu\frac{\partial^2 u}{\partial\xi_2^2}\right) \tag{A2}$$

v momentum:

$$\rho u\frac{\partial v}{\partial\xi_1} + \rho v\frac{\partial v}{\partial\xi_2} + \rho w\frac{\partial v}{\partial\xi_3} + \rho u^2\begin{Bmatrix}2\\1\ 1\end{Bmatrix} + 2\rho uv\begin{Bmatrix}2\\1\ 2\end{Bmatrix} + 2\rho uw\begin{Bmatrix}2\\1\ 3\end{Bmatrix} + \rho v^2\begin{Bmatrix}2\\2\ 2\end{Bmatrix} + 2\rho vw\begin{Bmatrix}2\\2\ 3\end{Bmatrix} + \rho w^2\begin{Bmatrix}2\\3\ 3\end{Bmatrix} + \frac{1}{g_{22}}\frac{\partial p}{\partial\xi_2} = 0 \tag{A3}$$

w momentum:

$$\rho u\frac{\partial w}{\partial\xi_1} + \rho v\frac{\partial w}{\partial\xi_2} + \rho w\frac{\partial w}{\partial\xi_3} + \rho u^2\begin{Bmatrix}3\\1\ 1\end{Bmatrix} + 2\rho uv\begin{Bmatrix}3\\1\ 2\end{Bmatrix} + 2\rho uw\{{}_1{}^3{}_3\} + \rho v^2\{{}_2{}^3{}_2\} + 2\rho vw\{{}_2{}^3{}_3\} + \rho w^2\{{}_3{}^3{}_3\} + \frac{g_{22}}{g}\left(g_{11}\frac{\partial p}{\partial\xi_3} - g_{13}\frac{\partial p}{\partial\xi_1}\right) = \frac{\epsilon^2}{g_{22}}\left(\frac{\partial\mu}{\partial\xi_2}\frac{\partial w}{\partial\xi_2} + \mu\frac{\partial^2 w}{\partial\xi_2^2}\right) \tag{A4}$$

Energy equation:

$$\rho u C_p\frac{\partial T}{\partial\xi_1} + \rho v C_p\frac{\partial T}{\partial\xi_2} + \rho w C_p\frac{\partial T}{\partial\xi_3} - \left(u\frac{\partial p}{\partial\xi_1} + v\frac{\partial p}{\partial\xi_2} + w\frac{\partial p}{\partial\xi_3}\right) = \frac{\epsilon^2}{g_{22}}\frac{\partial}{\partial\xi_2}\left(k\frac{\partial T}{\partial\xi_2}\right) + \epsilon^2\mu\left\{\frac{g_{11}}{g_{22}}\left(\frac{\partial u}{\partial\xi}\right)^2 + 2\frac{g_{13}}{g_{22}}\frac{\partial u}{\partial\xi_2}\frac{\partial w}{\partial\xi_2} + \frac{g_{33}}{g_{22}}\left(\frac{\partial w}{\partial\xi_2}\right)^2\right\} + \epsilon^2\left(\sum_{i=1}^{NS} C_{pi}\frac{\mu Le}{Pr}\frac{\partial C_i}{\partial\xi_2}\right)\frac{\partial T}{\partial\xi_2} - \sum_{i=1}^{NS} h_i\dot{w}_i \tag{A5}$$

Species continuity:

$$\rho u\frac{\partial C_i}{\partial\xi_1} + \rho v\frac{\partial C_i}{\partial\xi_2} + \rho w\frac{\partial C_i}{\partial\xi_3} = \frac{\epsilon^2}{g_{22}}\frac{\partial}{\partial\xi_2}\left(\frac{\mu Le}{Pr}\frac{\partial C_i}{\partial\xi_2}\right) + \dot{w} \tag{A6}$$

Equation of state:

$$p = \frac{\rho RT}{MC_{p\infty}} \tag{A7}$$

Appendix B: Nonequilibrium Shock-Crossing Relations

$$\hat{u}_{sh} = \frac{\cos\sigma}{1 + \dfrac{\epsilon^2}{n_{sh}}\dfrac{\mu_{sh}}{\sin\sigma}\left(\dfrac{\partial\hat{u}}{\partial\eta}\right)} \tag{B1}$$

$$T_{sh} = \frac{0.5(\hat{u}_{sh} - \cos\sigma)^2 + 0.5(\sin^2\sigma - \hat{v}_{sh}^2) + \sum_{i=1}^{NS} C_{i_\infty} h_{i_\infty}}{\sum_{i=1}^{NS} C_{i_\infty}\left(\frac{h_{i_{sh}}}{T_{sh}}\right) + \frac{\epsilon^2 k_{sh}}{n_{sh}\sin\sigma}\left(\frac{\partial \overline{T}}{\partial \eta}\right)} \tag{B2}$$

$$p_{sh} = \frac{p_\infty}{\rho_\infty U_\infty^2} + \sin\sigma(\hat{v}_{sh} + \sin\sigma) \tag{B3}$$

$$\rho_{sh} = \frac{p_{sh}}{T_{sh}\left(\frac{R}{C_{p_{ref}}}\right)} \tag{B4}$$

$$\hat{v}_{sh} = -\frac{\sin\sigma}{\rho_{sh}} \tag{B5}$$

$$C_{i_{sh}} = C_{i_\infty} - \epsilon^2\left(\frac{\mu Le}{Pr}\right)_{sh} \frac{1}{n_{sh}} \frac{\partial C_i}{\partial \eta} \frac{1}{\sin\sigma} \tag{B6}$$

References

[1] Miner, E.W. and Lewis, C.H., "Hypersonic Ionizing Air Viscous Shock-Layer Flows over Nonanalytic Blunt Bodies," NASA CR-2550, May 1975.

[2] Shinn, J.L., Moss, J.N., and Simmonds, A.L., "Viscous Shock-Layer Heating Analysis for the Shuttle Windward Plane with Surface Finite Catalytic Recombination Rates," AIAA Paper 82-0842, June 1982.

[3] Rakich, J.V. and Lanfranco, M.J., "Numerical Computation of Space Shuttle Laminar Heating and Surface Streamlines," *Journal of Spacecraft and Rockets,* Vol. 14, May 1977, pp. 265-272.

[4] Rakich, J.V., Stewart, D.A., and Lanfranco, M.J., "Results of a Flight Experiment on the Catalytic Efficiency of the Space Shuttle Heat Shield," AIAA Paper 82-0944, June 1982.

[5] Scott, C.D. and Derry, S.M., "Catalytic Recombination and the Space Shuttle Heating," AIAA Paper 82-0841, June 1982.

[6] Szema, K.Y. and Lewis, C.H., "Three-Dimensional Viscous Shock-Layer Flows Over Lifting Bodies at High Angles of Attack," AIAA Paper 81-1146, June 1981.

[7] Blottner, F.G., Johnson, M., and Ellis, M., "Chemically Reacting Viscous Flow Program for Multi-Component Gas Mixtures," Sandia Laboratories, Rept. SC-RR-70-754, Albuquerque, N. Mex., Dec. 1971.

[8] Helliwell, W.S., Dickinson, R.P., and Lubard, S.C., "Viscous Flow over Arbitrary Geometries at High Angle of Attack," AIAA Paper 80-0064, Jan. 1980.

[9] Murray, A.L. and Lewis, C.H., "Hypersonic Three-Dimensional Viscous Shock-Layer Flow over Blunt Bodies," *AIAA Journal,* Vol. 16, Dec. 1978, pp. 1279-1286.

[10] Weilmuenster, K.J. and Hamilton, H.H. II, "A Method for Computation of Inviscid Three-Dimensional Flow Over Blunt Bodies Having Large Embedded Subsonic Regions," AIAA Paper 81-1203, June 1981.

[11] Bird, R.B., Stewart, W.E., and Lightfoot, E.N., *Transport Phenomena,* John Wiley and Sons, Inc., N.Y., 1960.

[12] Davis, R.T., "Numerical Solution of the Hypersonic Viscous Shock-Layer Equations," *AIAA Journal,* Vol. 8, May 1970, pp. 843-851.

[13] Browne, W.G., "Thermodynamic Properties of Some Atoms and Atomic Ions," General Electric Co., Philadelphia, Pa., MSD Engineering Physics TM2, 1962.

[14] Browne, W.G., "Thermodynamic Properties of Some Diatomic and Linear Polyatomic Molecules," General Electric Co., Philadelphia, Pa., MSD Engineeering Physics TM3, 1962.

[15] Browne, W.G., "Thermodynamic Properties of Some Diatoms and Diatomic Ions at High Temperature," General Electric Co., Philadelphia, Pa., Aerospace Physics TM8, May 1962.

[16] Blottner, F.G., "Non-equilibrium Laminar Boundary-Layer Flow of Ionized Air," General Electric Co., Philadelphia, Pa., Rept. R64SD56, Nov. 1964.

[17] Armaly, B.F. and Sutton, K., "Viscosity of Multicomponent Partially Ionized Gas Mixtures Associated with Jovian Entry," *Aerothermodynamics and Planetary Entry, Progress in Astronautics and Aeronautics,* Vol. 77, edited by A.L. Crosbie, AIAA, New York, 1981, pp. 335-350.

[18] Armaly, B.F. and Sutton, K., "Thermal Conductivity of Partially Ionized Gas Mixtures," *Thermophysics of Atmospheric Entry, Progress in Astronautics and Aeronautics,* Vol. 82, edited by Thomas E. Horton, AIAA, New York, 1982, pp. 53-67.

[19] Throckmorton, D.A., "Benchmark Aerodynamic Heat Transfer Data from the First Flight of the Space Shuttle Orbiter," AIAA Paper 82-0003, Jan. 1982.

[20] Thareja, R., Szema, K.Y., and Lewis, C.H., "Viscous Shock-Layer Predictions for Hypersonic Laminar or Turbulent Flows in Chemical Equilibrium over the Windward Surface of a Shuttle-Like Vehicle," AIAA Paper 82-0201, Jan. 1982.

[21] Swaminathan, S., Kim, M.D., and Lewis, C.H., "Nonequilibrium Viscous Shock-Layer Flows over Blunt Sphere-Cones at Angle-of-Attack," AIAA Paper 82-0825, June 1982.